

A Study Of Graphene Oxide And Its Application In Biomedical

Dhulfiqar Ali Jeryo¹, Dr. G. Giridhar², Dr. Sandhya Cole³

¹P.G. Scholar, ²Assistant Professor, ³Head of the Department
^{1,2,3} Department Of Nanotechnology

^{1,2,3} Acharya Nagarjuna University, Nagarjuna Nagar, Guntur, A.P., INDIA

Email:- ¹dhulfiqar.92@gmail.com, ³sandhya.cole@gmail.com

Abstract

Graphene, a single layer of sp²-bonded carbon atoms has recently become a huge interest that acts as potential nanomaterials due to its advantages and unique sensory properties. The incorporation of metal nanoparticles on graphene as nanocomposite has been reported to significantly improved the material properties through surface modification. Hence, the development of the graphene-based nanocomposites has demonstrated excellent potential in the fabrication of highly sensitive sensors. A simple, cheaper, and reproducible technique to prepare graphene-based metal nanocomposites on a large volume is required in order to achieve successful incorporation of metal nanoparticles onto graphene-based materials. Therefore, a novel, easy to handle, less-toxicity, and high yield production of graphene oxide/graphene-based metal nanocomposites has been successfully designed. "Graphene may be the most remarkable substance ever discovered. But what's it for?"- John Colapinto, a staff writer at The New Yorker.

Keywords:- Graphene, Sp²-bonded, Carbon, Atoms, Nanoparticles,

Introduction

After Andre Geim, a physics professor at the University of Manchester, and a colleague Kostya Novoselov discovered an unusual new material called graphene; he wrote a three-page paper describing their discoveries.

It was twice rejected by the journal Nature, where reviewers stated that isolating a stable, two-dimensional material is impossible and that it was not a sufficient scientific advance. Indeed, in 2004 the paper, "Electric Field Effect in Atomically Thin Carbon Films" was published in Science, and it astonished scientists - science fiction had become reality¹.

Graphene, the two-dimensional sp²-hybridised carbon, is currently the most intensively studied material. This single-atom-thick sheet of carbon atoms situated in a honeycomb pattern is the world's strongest and thinnest material, also being an excellent conductor of both electricity and heat. From the application viewpoint, this two-dimensional material is considered to be more promising than other nanostructured carbon allotropes (1- dimensional nanotubes or 0-dimensional fullerenes)². The intensive research about graphene in recent years is promising a revolution in chemical and electrical engineering. Chemical Engineering of graphene-based materials applies physical sciences (nanographene for improving drilling fluids performance, integrated graphene dispersion to create high performance fluids, graphene-enhanced composites added to rubber to increase its strength, conductivity and impermeability, etc.) and life sciences. The bio-applications of graphene and its derivatives is due to many desirable properties, such as a high specific surface area (2,630 m²/g), mechanical strength (Young's

modulus, ~1,100 GPa), electrical conductivity (200,000 cm² V⁻¹ s⁻¹), thermal conductivity (~5,000 W/m/K) of graphene and bio-compatibility, low cost, scalable production and facile biological/chemical functionalisation of GO³. Graphene oxide easily combines with many other nanoscale materials leading to new applications in the fields of drug delivery, cancer therapeutics, tissue engineering, diagnostics and bioimaging⁴.

Carbon materials

Carbon can be found in some common gases. When it reacts with oxygen, it can form carbon dioxide (CO₂). This is the scientific name for the gas we release from our bodies every time we exhale. Most important, carbon is found in every living thing. From dinosaurs to dogs, carbon is a component of all life, both past and present. All forms of life, including numerous things we use every day, owe their existence to a form of carbon. Mankind has known of carbon for centuries, but no single person is credited with discovering this element or giving carbon its name. The word "carbon" comes from the Latin word "carbo", meaning ember or charcoal. Because fire was one of the first things humankind ever knew, fire remnants - soot and charcoal - were very common in the ancient lifestyle and thus were also named carbo. When a natural item that contains carbon, such as wood, is burned, carbon becomes concentrated as soot, charcoal and ash. Soot, charcoal, and ash are forms of carbon called amorphous carbon. The ancient Greeks first developed the concept of an element. They claimed that everything was made up of at least one of the four elements - earth, air, fire, and water. In the mid-seventeenth century, British philosopher and chemist Robert Boyle agreed with the idea that there are basic elements that make up everything. But Boyle claimed there are many more than these four elements. Boyle theorized that

everything was made up of every small particle of matter. Matter is anything that has mass and takes up space. Boyle concluded that these particles of matter could only be differentiated by their shape and motion. These particles, classified by their differing shapes and motions, became known as elements. Boyle is often associated with the identification of carbon as an element. But it would take other scientists, including Englishman Sir Humphrey Davy, to show that coal, soot, charcoal, and diamond were all versions of the same element - carbon. After carbon was identified, scientists later realized that it can be either the hardest or one of the softest substances, depending on its form.

The carbon atom, with its six electrons, is tetravalent, having four of the electrons available for chemical bonding. Because of the flexibility of its bonding, carbon has several different allotropes with a large variety of physical properties. The main forms of elemental carbon are diamond and graphite. Under ambient conditions graphite is the stable phase, while under the application of high pressure and high temperature a transformation to the diamond structure occurs².

The Anatomy of an Element

An element is one of the more than 100 known substances that cannot be separated into a simpler substance by physical or chemical means.

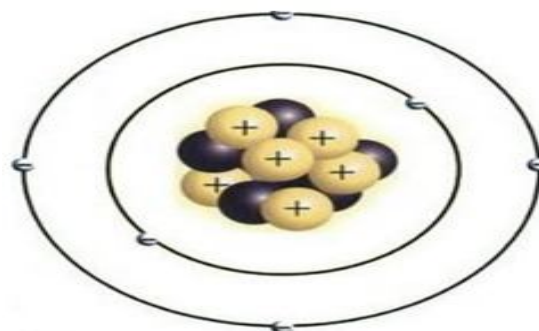


Fig 1. Nucleus of Carbon Atom

The nucleus of the carbon atom contains six positively charged protons and six neutrons, which have no charge. Surrounding the nucleus are two shells of negatively charged electrons. The first shell contains two electrons, while the second contains four. The carbon atom has room to add four more electrons to its outer shell.

Subatomic Particles

Until the early twentieth century, scientists believed the atom was the smallest structure known to mankind. That was until scientists realized that atoms have structure too. The main particles that make up atoms are protons, neutrons, and electrons. These are called subatomic particles. Protons have a positive electric charge; neutrons have no charge; and electrons have a negative electric charge. All atoms contains a nucleus, or center, where the protons and neutrons are contained.

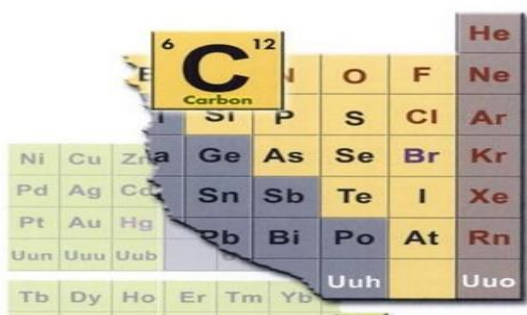


Fig 1.1: Periodic Table of Carbon

Carbon is found in Group IV of the periodic table and has atomic number 6. All element are made up of tiny units called atoms, which can only be seen using extremely powerful microscopes. Inside the atoms are minute particle: positively charged electrons, and neutrons, which do not have any charge. The atomic number tells us how many protons that are in each atoms of an element, so carbon atoms contains six protons.

Carbon has been assigned the chemical symbol “C” on the periodic table. The number in the upper left corner represents the atomic number, or the number of protons

the elements contains. The number in the upper right corner represents the element’s atomic weight.

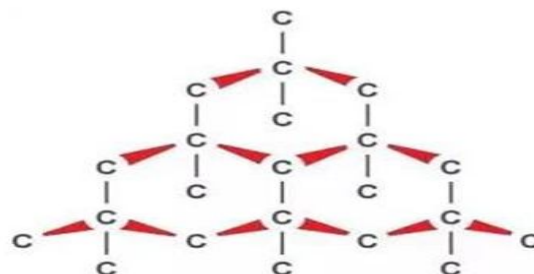


Fig 1.4 : This sparkling diamond is one of the naturally occurring forms of carbon

In a diamond, each carbon atom makes four strong bonds with four other carbon atoms. The atoms are arranged in a shape called tetrahedron. The strong bond makes diamond very hard. In fact, it is the hardest known natural substance.

A Stable arrangement

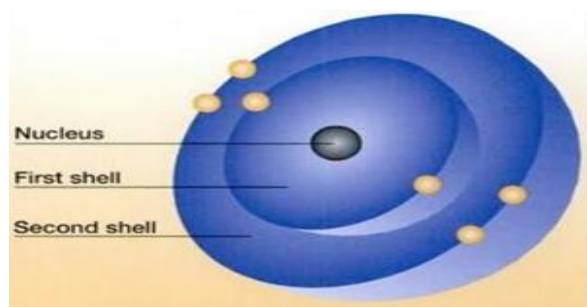
Atoms are only stable if their outer electron shell is full. The gain, loses, or share electrons with other atoms so that all the atoms involved end up with complete outer shells. As the atoms transfer or share electrons in a reaction, they form bonds between each other, resulting in molecules and compounds.

Each element has an atomic mass, which is the number of protons and neutrons added together. Carbon has six protons and six neutrons. This gives an atomic mass of 12.

Carbon and its compounds

Carbon is very reactive. It forms a huge number of compounds with many other

elements. Compounds containing carbon outnumber the compounds of all the other elements. The study of organic, or carbon based, chemistry is one of the most important areas of science. As well as joining with other elements, carbon atoms can also form strong bonds with up to four other carbon atoms. This produces rings or chains, which can be many thousand of atoms long.



Carbon also has three crystalline forms, in which each atoms bond with its neighbors to create a regular, repeating pattern. Two of these forms have been known for many hundreds of years. The third has also recently been discovered, and scientists are still finding out about its properties and possible uses. These different crystalline forms are called allotropes of carbon.

Scientists measure the radioactivity and use it to find the age of objects that contain dead plant or animal material. This process is called carbon dating. It has been used to find the age of wooden ornaments, boats that have lain at the bottom of the ocean for hundreds of years and the remains of prehistoric plants, animals, and people. Each carbon atoms contains a nucleus and two shells of electrons. There are two electrons in the first shell and four in the second shell.

MATERIALS AND RESEARCH METHODOLOGY

Materials

All reagents used in the experiments were chemically or analytically pure commercial reagents. The experiments with cells were carried out in vitro with Chinese hamster

ovary (CHO) and mouse hepatoma MH-22A (MH-22A) cell lines. The preparation and estimation of CHO and MH-22A cell viability were performed.

Table 3.1. List of reagents used

Reagent	Formula
Graphene oxide. Highly concentrated graphene oxide dispersion in water; 500 mg/l.	$C_xO_yH_z$
The high-quality CVD graphene films with coverage of about 95% of Si/SiO ₂ substrates	C_x
Meso-tetra (4-sulfonatophenyl) porphine dihydrochloride (TPPS ₄) Mass: 1007.92; purity: >95%	$C_{44}H_{32}N_4O_{12}S_4Cl_2$
Fe(III) meso-tetra (4-sulfonatophenyl) porphine chloride (FeTPPS ₄) Mass: 1024.27; purity: >95%	$C_{44}H_{28}FeN_4O_{12}S_4Cl$
Hematoporphyrin IX dihydrochloride (HP). Mass: 671.61; purity: >95%	$C_{34}H_{40}Cl_2N_4O_6$
Meso-tetra (4-pyridyl) porphine (TPyP) Mass: 618.70; purity: >97%	$C_{40}H_{26}N_8$

3.1 Methods

Preparation of graphene oxide

The graphene oxide (GO) dispersion was prepared by diluting dispersion, with a concentration of 500 mg/l with deionised water. Before using it for the experiments, the GO dispersion was sonicated for 1 hour in an ultrasonication bath (Branson 2510, USA).

For the Raman scattering and AFM measurements a drop of dispersion was dropped onto glass or another substrate and it was left to dry for 1 h. The functionalisation of graphene with meso-tetra (4-sulfonatophenyl) porphyrins

Coverage of the purchased high-quality CVD graphene film on Si/SiO₂ substrates was 95%. The thickness of the SiO₂ layer was 285 nm. The metal-free and Fe (III) meso-tetra (4-sulfonatophenyl) porphyrin solutions (TPPS₄ and FeTPPS₄, respectively) (10⁻⁵ M concentration) were

prepared by dissolving in deionised water of TPPS4 and FeTPPS4 porphine chloride powders. The reversible protonation/deprotonation process of metal-free TPPS4 is performed by adding HCl or NaOH into the stock solution and controlled by both pH measurements (pH-150 M, Gomel Plant of Measuring Devices) and direct UV-Vis characterisation. Before the adsorption of porphyrins on graphene, the solutions were filtered through 200- nm pore membrane filters, then precipitated onto the substrates by the drop-and- dry method (5 μ l per a droplet) and rinsed for 5 min with deionised water.

The functionalisation of graphene oxide with hematoporphyrin

The GO stock dispersion was prepared by diluting 510 μ l GO (500 mg/l) in 500 μ l deionized water. For the preparation of acidic solutions, a few μ l of concentrated sulfuric acid (SA) were added to the stock dispersion of GO to reach a final pH value of c.a. 2.0. The hematoporphyrin solution was prepared by diluting 500 μ l HP (10-5 M concentration) in 500 μ l deionized water. For acidic solutions of HP, conc. sulfuric acid was added to reach the pH value of the final solution of c.a. 2.6. The reversible esterification reaction is performed by adding SA or NaOH into the solution and controlled by pH measurements at room temperature and direct UV-Vis characterisation. For the Raman scattering and FT-IR measurements a drop of dispersion was placed on the glass substrate; in the case of Raman scattering it was left to dry for 1h.

Measurements concept and data processing algorithms

Initial measurements were focused on the properties and aggregation state of single HP and GO itself under sulfuric acid treatment.

Then, the interaction between hematoporphyrin and graphene oxide was measured at neutral pH. Finally, hematoporphyrin, graphene oxide and sulfuric acid interactions were investigated. In the last case, the reversibility of the reaction between hematoporphyrin and graphene oxide was controlled by UV-Vis measurements using H₂SO₄ and NaOH water solutions for pH changing. Measurements for different GO- HP ratios were performed in line with the following procedure: 1:10 diluted initial solutions of HP (10-5 M) were mixed with the same volume, but different concentrations of GO (500 mg/l) water solutions -1:2, 1:5, 1:10, 1:12.75, 1:20 (by volume). Fluorescence measurements were undertaken using a USB2000 fibre optic spectrometer, excited by blue laser (473 nm). The same measurements were also repeated for samples with the addition of 1 μ l of conc. H₂SO₄ (pH 2). The total emission was calculated in the following way:

$$I^*(t) = \sum_{\lambda=600\text{ nm}}^{\lambda=700\text{ nm}} I(t) \quad (3.1)$$

where $I(t)$ is the intensity of average and background corrected luminescence response.

The HP/GO ratio γ (surface/surface) within aggregates was estimated using the following procedure. The total surface area occupied by the HP molecules and GO flakes are designated as SHP and SGO, respectively. Hence, the HP/GO ratio γ might be described by the following expression:

$$\gamma = \frac{S_{HP}}{S_{GO}} \quad (3.2)$$

SHP and SGO are the total surface areas occupied by the HP molecules and GO flakes, respectively. SGO might be easily estimated using a value of graphene oxide specific surface area δ specified by the producer (c.a. 833 m² /g) contrary to the

same value of graphene in 2,630 m²/g 80. If x_{GO} (gram) is the total mass of GO in solution, the surface area covered with GO is expressed by the formula:

where mw_{HP} (gram) = 598.69 g and N_A = 6.0221•10²³ are the molecular weight of HP and Avogadro number respectively. When S_{HP} and S_{GO} are expressed from (3.2) and (3.3) equation (3.4) becomes:

$$\gamma = \frac{S_{HP}}{S_{GO}} = \frac{x_{HP}}{x_{GO}} \cdot \frac{s \cdot N_A}{\delta \cdot mw_{HP}} \approx 2 \cdot \frac{x_{HP}}{x_{GO}} \quad (3.5)$$

It is reasonable to stress that the value of γ (surface/surface) is slightly underestimated owing to the overestimation of s and underestimation of δ . The analysis of concentration dependences was performed in the framework of the competition model using the Morgan- Mercer-Flodin equation or the logistic curve for data in the steady-state regime (Snopok, Boltovets and Rowell, 2006):

$$I^* \sim \frac{1}{1 + (\frac{\gamma}{\gamma_0})^p} \quad (3.6)$$

$\gamma \sim 1/x_{GO}$ and $\gamma_0 \sim 1/x_{HP}$, where X_{HP} is the initial amount of the competitor (HP) in the solution and x_{GO} is proportional to the total value of adsorbed capacity of GO. Power p represents the order of the reaction in the competitor (HP), an effective value indicating the mechanism of the processes occurring in the system. To approximate the curves and linear dependence, the nonlinear regression analysis procedures of OriginPro 8.5 were used.

The functionalisation of graphene oxide with meso-tetra (4-pyridyl) porphine

Meso-tetra (4-pyridyl) porphine was dissolved in deionised water at room temperature under acidic aqueous medium (HCl was added to reach pH 2 at the concentration 5x10⁻⁴ M), obtaining a

greenish colloid. Graphene oxide dispersion, with a concentration of 500 mg/l was diluted with deionised water. A suspension of aggregates was prepared by a simple π - π stacking approach. The pH was adjusted using HCl solution to reach 1.5 to 2.3 pH and 1% CaCO₃ to reach a pH from 5.4 to 9.1. In a typical experiment, GO was suspended in anionic meso-tetra (4-sulfonatophenyl) porphine dihydrochloride aqueous solution. Measurements of the absorption and fluorescence spectra were carried out after mixing 5x10⁻⁴ M porphyrin with different concentrations of graphene oxide at room temperature within 1 min. For the Raman scattering and AFM measurements a drop of solution was placed on the glass/gold substrate and left to dry for 1 h

The functionalisation of graphene oxide with doxorubicin

Doxorubicin (DOX) was dissolved in deionised water to obtaining a concentration of 0.05 μ g/ml. Sonicated graphene oxide dispersion (500 mg/l) was diluted with deionised water to obtaining a concentration of 6.25 μ g/ml and mixed with doxorubicin.

For the experiments with an additionally heated mixture, the prepared suspension was placed in an ultrasonication bath for additional 1 hour with heating (~40°C) to catalyse a covalent bonding between the GO carboxyl and DOX amino groups.

Substrate preparation

For the AFM, SEM and Raman measurements substrates were immersed in the Piranha solution for 24 h and after that rinsed a few times with deionised water. As support for the lipid bilayers, glass coverslips were used. The pieces (ca. 2.5 × 4 cm) were cleaned in ethanol and sonicated for 15 min at 20°C in an ultrasonic bath and stored in ethanol. Before use, substrates were rinsed several times with deionised water, dried with nitrogen gas, affected with low pressure

plasma (Electronic Diener) for 10 minutes and glued onto an aluminium sample cell.
Preparation of bilayer lipid membrane

Bilayer lipid membranes were prepared following a modified protocol of Richter et al (2003). The mixture of phospholipids: DOPS, DOPC and DOPE were solved in chloroform and mixed at a ratio of 35:65:0.000016. If DOPE were not used, the DOPS and DOPC ratio was 35:65. The lipid was dried overnight under vacuum to remove the solvent and then resuspended in Tris buffer (149 mM NaCl, 5 mM CaCl₂, 10 mM Tris) to a final concentration of 0.1 g/l. The resulting solution was extruded 27-29 times through a membrane (pore size 0.1 μm) to produce unilamellar vesicles. The vesicle solution was put directly in the measurement cell containing the glass substrate. The lipid solution was flooded with a peristaltic pump for 10 min with a velocity of 0.250 ml/min, then the solution was left for 20 min so the vesicles could disperse on the surface, and after that it was replaced by the pure Tris buffer. Subsequently, this solution was exchanged again by a Ca²⁺ free Tris buffer (10 mM Tris, 133 mM NaCl) containing 5 mM EDTA in order to remove the Ca²⁺ ions and finally by PBS buffer. All buffers contained 0.05% NaN₃ and were adjusted to pH-7.4. After 3 h of rinsing with PBS, the bilayer was ready for measurements with other nanoparticles.

For the Raman measurements, bilayer lipid membranes were prepared in the following way: the mixture of phospholipids, DOPS and DOPC, were solved in chloroform and mixed at a ratio of 35:65. The lipids were dried with nitrogen gas and then resuspended in Tris buffer to a final concentration of 0.1 g/l. The resulting solution was extruded 27-29 times through a membrane (pore size 0.1 μm). The vesicle solution was put directly on the SERS substrate. The lipid solution was left for 30

min and after that it was replaced by the pure Tris buffer. Then, this solution was exchanged after 15 min again by a Ca²⁺ free Tris buffer containing 5 mM EDTA in order to remove the Ca²⁺ ions and finally, after another 15 min - by PBS buffer. After 1 h of rinsing with PBS, the bilayer lipid membranes were ready for Raman measurements. For the analysis of the FCS data a diffusion model expanded by a second diffusion coefficient in a linear combination (D, D_a, D_b) was used.

$$G(\tau) = a * G_0 * \left(\frac{1 + 4 D_a}{\omega_0^2 \tau} \right)^{-1} + b * G_0 * \left(\frac{1 + 4 D_b}{\omega_0^2 \tau} \right)^{-1} \quad (3.7)$$

$$D = a * D_a + b * D_b \quad (3.8)$$

where G₀ is the intercept of the FCS curve and inverse proportional to the number of the fluorescent molecules and ω₀ is the radius of the detection volume.

Preparation of cell culture for experiments

The cells were cultured in 25 cm² tissue culture flasks in DMEM supplemented with 10% FBS, 1% L-glutamine, 90 μg/ml streptomycin and 100 U/ml penicillin (complete DMEM) in a humidified atmosphere of 95% air and 5% CO₂ at 37°C. When the cells reached confluence, they were detached from the bottom of the flask with 1.5 ml of 0.25% trypsin- 0.02% EDTA solution. Then, the cell suspension was supplemented with 2.5 ml of complete DMEM, centrifuged for 2 min at 1,000 rpm (Biosan LMC-3000, Latvia) and resuspended in 1 ml of complete DMEM.

The preparation of sample and estimation of cell viability

The 10% BSA solution was prepared by diluting BSA in 0.9% NaCl. The influence of GO and GO-BSA on the viability of CHO and MH-22A cells was evaluated by a colony formation assay (Freshney, 2005). 40

mm diameter Petri dishes were filled with 2 ml of complete DMEM, which was afterwards supplemented with the corresponding investigating materials (one of the following: 10% BSA; 12.5, 25.0 or 50.0 µg/ml of GO; 12.5, 25.0 or 50.0 µg/ml of GO with 10% BSA). Also, control samples (without GO and GO-BSA treatment) of CHO and MH-22A cells with 0.9% NaCl solution were prepared. The Petri dishes were incubated for 30 min under the same conditions as described above. Approximately 300 cells per Petri dish were seeded. Then, the cells were incubated for 5 (CHO) or 8 (MH-22A) days for the formation of colonies. After incubation the cell colonies were fixed using 70% ethanol. After fixation, the cells were stained with a Gram's crystal violet solution, air dried and counted through a binocular light microscope with 16x magnification. The viability of experimental groups was expressed as a percentage number of colonies compared to control (100%). Digital images of the colony examples were taken using a Moticom 2300 camera (Motic, Hong Kong) which was connected to the inverted ECLIPSE TS100 microscope (Nikon, Japan) with a magnification of 40x.

The preparation of cell samples for investigation by AFM and Raman spectroscopy and imaging

100 µl of the cells suspension (1x10⁶ cells/ml) was seeded on the surface of a lithium niobate plate into each Petri dish filled with 2 ml of complete DMEM. The lithium niobate plates were selected because of good surface characteristics for cells growth and for the following analysis by Raman spectroscopy because of low background signal. Then the cells were incubated for 24 h (CHO) or 48 h (MH-22A) to reach a confluent cell monolayer. Controls, without the treatment with GO, were performed in the case of both cell lines. GO dispersion was sonicated as described

above. GO (12.5 µg/ml) was added into the Petri dishes with the cells for further incubation. After 24 h incubation the cells were washed with deionised water, fixed with 4% formaldehyde (in PBS) for 10 min at room temperature, washed again with deionised water and air dried⁸¹.

Analytical techniques

In this thesis, a number of analytical techniques have been used with the aim to characterise the final products and to identify important experimental parameters. Raman spectroscopy has been used to obtain an understanding of the chemical composition, and atomic force microscopy giving the information about the morphology of the sample. Other methods applied in this work are UV-Vis, supercritical angle fluorescence and Fourier transform infrared spectroscopies, and scanning electron and light microscopies

Raman spectroscopy

The Raman measurements were undertaken using the NTEGRA Spectra system (NT-MDT Inc.) in an upright configuration. The excitation wavelength was 532 nm (20-mW DPSS laser, LCM-S-111-20-NP25) with a controlling laser power in the range of 0.005–5 mW. To avoid extensive heating of the sample and beam damage, a different laser power was used for the analysis. The instrument was equipped with a 100× 0.7 NA objective, resulting in a diameter spot of 0.5 µm at the laser focus. The beam was focused on the sample, which rests on a controlled XYZ piezo stage capable of scanning samples over 130 × 130 × 7 µm. The scattered light was collected by the same objective and directed through a 100-µm pinhole into a spectrometer (Solar TII, MS5004i). The signals were analysed with a TE-cooled (60°C) CCD (1,024 × 128 pixels, DV401- BV, Andor Technology). The diffraction gratings of 600 lines/mm or 1,800 lines/mm were used, resulting in a spectral resolution of about 2.5 cm⁻¹ or 0.8

cm-1, respectively. Another CCD is used to collect bright field images. A confocal Raman system was also used for measurements in a water environment.

The Raman measurements of cells were measured as follows: The search for GO in the cells was performed by the estimation of the characteristic Raman spectrum, the series of Raman spectra were recorded consistently along the Z axis across the cell, starting from outside of the cell. Over 260 spectra from 24 different cells were evaluated, and at least 11 spectra were acquired from each cell. The power of the laser at the sample was 5 mW for CHO and 0.5 mW for MH-22A, acquisition time - 5 s. To avoid overheating, a different power of laser irradiation at the cells was used. The distribution of GO inside the cells and cell fingerprint spectra were monitored by Raman imaging. Laser power was 5 mW at the cell surface, acquisition time - 1 s/pixel, image resolution - 92 x 92 pixels. Hyperspectral image collect over 8,000 spectra from each mapping picture. The GO distribution inside the cells was investigated by collected spectra evaluation and GO spectra map building on top of the confocal optical cell image.

Atomic force microscopy

Measurements were performed using NT-MDT Solver system (NT-MDT Inc.) in a semi- contact mode using commercial silicon cantilevers with a tip diameter of 10 nm and a force constant of 1.5 N/m. The AFM investigations for the ZnO and TiO₂ nanoparticles were done using commercial silicon cantilevers NSG11 with a force constant of 5 N/m.

The morphology of the supported lipid membranes was investigated by AFM imaging. Measurements were performed using the NT-MDT Solver system (NT-MDT Inc.) in a semi- contact mode in solution using commercial silicon cantilevers with a

resonant frequency of 7-20 kHz and a spring constant of 0.08 N/m. Images were processed and analysed with NTEGRA Spectra software.

Cells morphology was investigated by AFM imaging and measurements of the cells membrane roughness. Measurements were performed for both cell lines using NT-MDT Solver system (NT-MDT Inc.) in a semi-contact mode using commercial silicon cantilevers with a tip diameter of 10 nm and force constant 1.5 N/m. Cell membrane roughness was measured on the topography images using SPIP™ software. The roughness average (SA) parameter was used for the comparison of the measured topographic results. Thirty surface areas of the cells (1000 × 1000 nm) were chosen at random from three independent experiments for CHO control cells, mouse hepatoma MH-22A control cells, CHO cells after the treatment with 12.5 µg/ml of GO and mouse hepatoma MH-22A cells after the treatment with 12.5 µg/ml of GO.

Supercritical angle fluorescence spectroscopy

SAF is a technique to detect and characterise fluorescent species (proteins, biomolecules, pharmaceuticals, etc.) and their behaviour very close or even adsorbed or linked to surfaces. The method is able to observe molecules at a distance of less than 100 nanometre from the surface even in the presence of high concentrations of fluorescent species. Using an aspheric lens for excitation of a sample with laser light, fluorescence emitted by the specimen is collected above the critical angle of total internal reflection selectively and directed by parabolic optics onto a detector (Fig. 3.2). The method was invented in 1998 in the laboratories of Stefan Seeger at the University of Regensburg (Germany) and later at the University of Zurich

(Switzerland)82. The principle on how SAF microscopy works is as follows. A fluorescent specimen does not emit fluorescence isotropically when it comes close to a surface, but approximately 70% of the fluorescence emitted is directed into the solid phase. Here, the main part enters the solid body above the critical angle. When the emitter is located just 200 nm above the surface, fluorescent light entering the solid body above the critical angle is decreased dramatically. Hence, SAF Microscopy is ideally suited to discriminating between molecules and particles at or close to surfaces and all other specimen present in the bulk (Ruckstuhl, Rankl and Seeger, 2003).

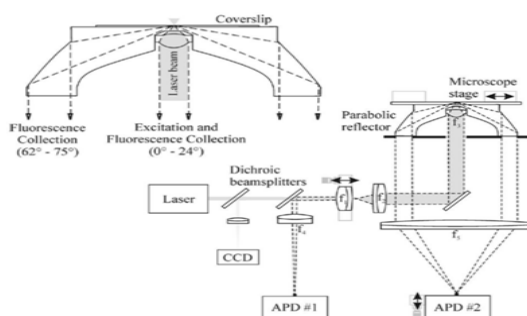


Fig. 3.2. Setup of SAF microscope (Ruckstuhl, Verdes, 2004)

Images of fluorescently labelled lipid membranes were recorded with a custom-made scanning microscope allowing the detection of fluorescence and the supercritical angle fluorescence images of an emitter simultaneously. The SAF channel detects only fluorophores in close proximity to the surface (~100-200 nm) and efficiently rejects the fluorescence from the bulk solution using parabolic lenses as the decisive optical element. All measurements were conducted by passing buffered solutions of NP's over the lipid membrane through the flow cell at a constant pump rate of 250 $\mu\text{l}/\text{min}$ (0.42 mm/s) (Fig. 3.3). This flow rate is clearly slow enough to have no effect on the bilayer lipid membrane integrity. Raw scan images are presented as measured using an appropriate linear scaling

for the signal intensities. Note that the background subtraction in all images is based on a fixed intensity threshold. The shown images are selected representative images from time-lapse experiments which were conducted at varying time intervals because the applied setup (non-commercial) does not contain the option of a software controlled time-lapse measurement.

Fluorescence correlation spectroscopy (FCS) is a method that was introduced and established as a very suitable approach to characterise membranes 83 . FCS was employed by several authors to measure the lateral lipid mobility and to assess the impact of NP's on lipid dynamics in supported lipid membranes (Garcia-Saez, Carrer and Schwille, 2010; Garcia-Saez and Schwille, 2008).

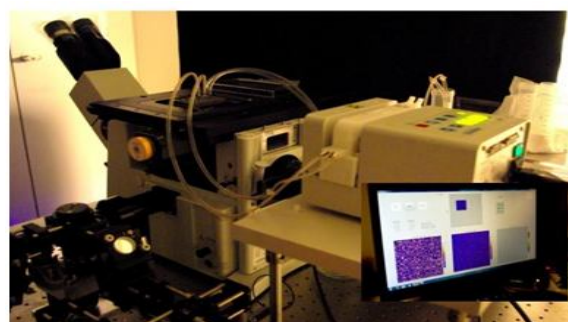


Fig. 3.3. Supported lipid bilayer formation on SAF microscopy

A hardware correlator translates the photon arrival pulses into intensity fluctuations and calculates the correlation real-time. The correlation curves were acquired and fitted to analytical expressions. For an averaged correlation measurement, a separate correlation measurement of 100 seconds duration was taken, and corresponding standard deviations for every point of the experimental curves were calculated from multiple experiments.

The diffusion coefficient of the lipids in the supported lipid bilayer was determined from the experimentally obtained correlation time

and the known waist of the confocal observation volume.

UV-Vis spectroscopy and emission spectra measurements

The principle of ultraviolet-visible absorption is that molecules containing π -electrons or non-bonding electrons (n-electrons) can absorb the energy in the form of ultraviolet or visible light to excite these electrons to higher anti-bonding molecular orbitals⁸⁴. The more easily excited the electrons (i.e. lower energy gap between the HOMO and the LUMO), the longer the wavelength of light it can absorb.

The absorption and emission spectra measurements were undertaken using a USB2000 fibre optic spectrometer (Ocean Optics). The fluorescence was excited by a 500 mW DPSSL laser (473 nm, LRS-476-TM-50-5, Laserglow Technologies)

Scanning electron microscope

A scanning electron microscope (SEM) produces images of a sample by scanning it with a focused beam of electrons. The electrons interact with atoms in the sample, producing various signals that contain information about the sample's surface topography and composition.

The morphology and composition of the aggregates were examined using a SEM/Focused Ion Beam (FIB) workstation Helios Nanolab 650 with an energy dispersive X-ray (EDX) spectrometer INCA Energy 350 X-Max 20.

Light microscopy

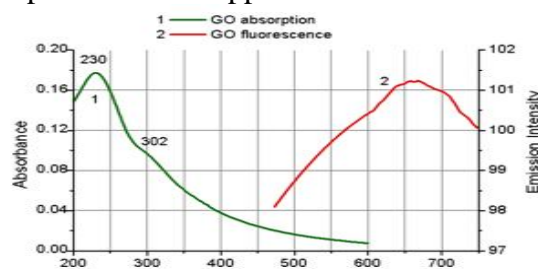
Digital images of the colony examples were taken using a Moticam 2300 camera (Motic, Hong Kong) which is connected to the inverted ECLIPSE TS100 microscope (Nikon, Japan) with 40x or 125x magnification.

RESULTS

The functionalisation of graphene/graphene oxide with organic molecules and characterisation

Characterisation of graphene oxide

The preparation of GO solution in neutral pH was carried out according to the procedure described in section 3.2.1. The UV-Vis measurements were performed in order to determine the formation of stable graphene dispersions. As shown in Fig. 4.1, the absorption peak of the GO dispersion at 230 nm and a weak shoulder at ~302 nm suggests that the electronic conjugation within the electronic conjugation level of graphene is chemically controllable, offering possibilities to tailor the properties of graphene sheets. Graphene sheets with different reduction levels can also form stable dispersions with other materials. In addition, GO is also expected to exhibit unique optical properties as evidenced by the recent demonstration of photoluminescence. This luminescence was found to occur from the near-UV-to-blue visible to near-infrared (IR) wavelength range⁸⁵. This property could be useful for biosensing, fluorescence tags and optoelectronics applications.



The illumination of GO samples was performed with blue laser (473 nm), so no near-UV-to-blue visible fluorescence was noticed, indeed, the low intensity luminescence within the range of 600-700 nm was induced. The shift in the fluorescence peaks of the suspension may be attributed to the differences of the surrounding medium. Pan et al. (2010) have

demonstrated that the blue fluorescence of graphene is pH-dependent. The fluorescence is strong enough to be observable by the naked eye at high pH levels, while it is nearly quenched in low pH levels. The explanation is that protonation of the emissive zigzag sites at acidic pH conditions quenches the fluorescence and deprotonation in alkaline conditions, recovers it⁸⁶.

GO characterisation with AFM

In order to explore the GO structure in more depth, microscopic techniques such as atomic force microscopy have been employed for the investigation of its structural features. AFM directly gives the apparent thickness of the single-layer GO (around 1 nm, fig. 4.2) as well as the number of layers.

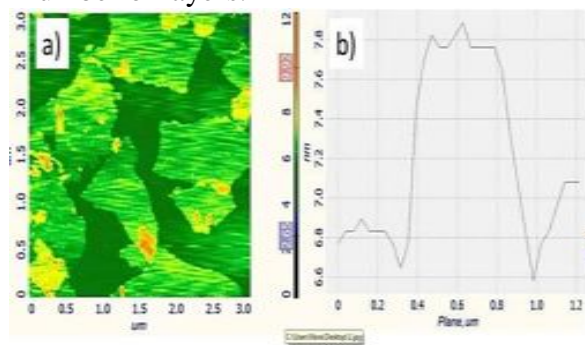


Fig. 4.2. GO characterisation by AFM. a) Height image of GO flakes b) cross section of a GO flake

To prove the impact of sonification for GO solution, the following experiment was performed. The different samples of a) GO sample without sonification b) GO after 30 min sonification and c) after 1 hour sonification were prepared by putting the solution of GO in a sonification bath for the corresponding time, then samples were dropped onto the mica surface and kept for 5 min, after that spin coating was performed. Samples were tested with AFM and the influence of the sonification time

was evaluated from the obtained pictures (Fig. 4.3).

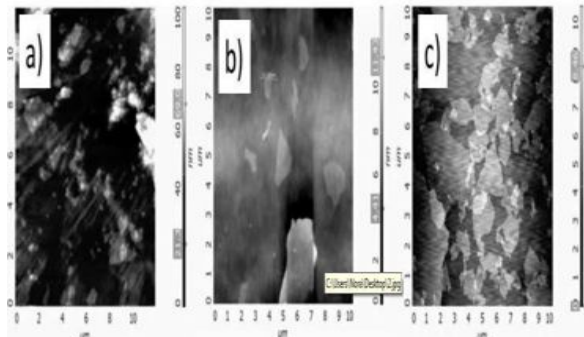


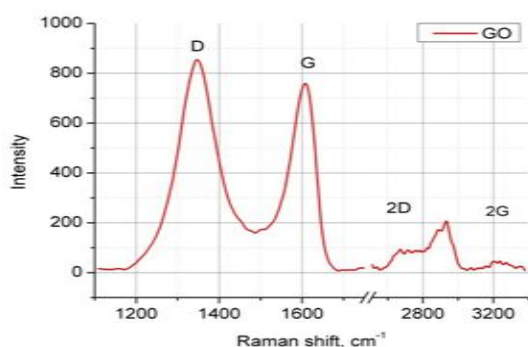
Fig. 4.3. GO characterisation with AFM. a) Without sonification, b) after 30 min sonification, c) GO after 1 hour sonification
 From the obtained AFM pictures after 1 hour sonification the small flakes of GO (0.3-0.7 μm) are dominant. After 30 min sonification, the middle size flakes (0.9-1.2 μm) are dominant. Without sonification, the big size flakes (1.2 μm and more) are dominant. According to the manufacturer data sheet (Graphene Supermarket) the size of flake is: 0.3-0.7 microns and a thickness of 1 atomic layer - at least 80%. So, before all experiments with GO solution, the sonification for at least 1 hour is needed to recover of characteristics provided by producer.

GO characterisation with Raman spectroscopy

Raman spectroscopy can be used for both quantitative and qualitative investigations. For example, the amount of layers (single layer, bilayer, etc.) of graphene and the effect of substrates on the graphene characteristics, etc. can be determined by Raman spectroscopy. The Raman spectrum of graphene oxide shows the main features of the carbon materials, D~1,334 cm^{-1} , G~1,559 cm^{-1} , 2G ~3,200 cm^{-1} and 2D (often also referred to as G) bands ~2,668 cm^{-1} (using an excitation wavelength of 532 nm). The G band is due to bond-stretching in rings and chains⁸⁷. The D band

is caused by the breathing modes of sp²-atoms in rings. The D-band appears when structural disorder, e.g. impurities and edges, breaks the translational symmetry. The D band intensity can be correlated to the edges and other defects in the graphene sheet⁸⁸. Thus, the G and D bands provide useful information on in-plane vibrations and defects, respectively. For graphite the D/G ratio has been related to the in-plane grain-size⁸⁹. This ratio gives a means to analyse the disorder in the graphene system. The 2D band gives information on the stacking order and has recently been used as a simple and efficient way to identify single layer graphene sheets. Raman spectroscopy was applied to graphene single layers, bilayers, etc. by different researchers⁹⁰. For single-layer graphene the relative intensity between the G and 2D band reverses as compared to multilayer flakes⁹¹. Moreover, other nanomaterials can also be characterized using Raman spectroscopy.

Fig. 4.3. The typical Raman spectra of GO (λ_{ex} - 532 nm)



The typical Raman scattering spectra of the measured GO films presented in Fig. 4.3. The typical band regions of the in-phase vibration of the GO lattice (G and 2G band) are at

~1,600/3,200 cm⁻¹ and the disorder band regions caused by the GO edges (D and 2D band) are at ~ 1,334/2,668 cm⁻¹.

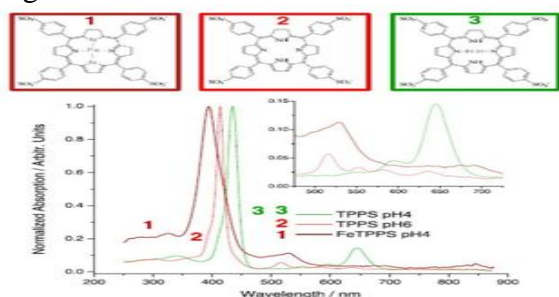
Graphene functionalisation with meso-tetra (4-sulfonatophenyl) porphines

A non-covalent interaction of iron and metal-free meso-tetra (4-sulfonatophenyl) porphines (FeTPPS4 and TPPS4) with single-layer graphene was investigated. The central metal atom of porphyrin macrocycle (iron) plays an important role in the integrity of FeTPPS4 on graphene surfaces. The interaction of metal-free TPPS4 with graphene leads to the deprotonation of TPPS4 molecules and not significant Raman enhancement values. The Raman enhancement factors were evaluated as a ratio of background subtracted Raman spectra of the corresponding films on graphene and glass multiplied by factor of 3 which is caused by the difference in the film thicknesses on glass (25 ± 5 nm) and graphene (8 ± 2 nm). For TPPS4 film (pH = 4) the enhancement factor of 4 is obtained for all peaks due to a strict conformity of the spectra (the deviation is ± 0.3). On the contrary, the Raman signals of FeTPPS on graphene are reduced by a factor of 1.5. Deprotonated TPPS4 solutions after the adsorption on the graphene surface demonstrates the appearance of new Raman bands (774, 1,181, 1,653 cm⁻¹) and enhanced Raman signals (1,363, 1,509 cm⁻¹). A strong non-covalent interaction between deprotonated TPPS4 and graphene is realised through pyrrole and desulphonated phenyl rings of closely located planar TPPS4 molecules on the graphene surface.

UV-Vis and Raman characterisation of TPPS/FeTPPS porphyrins

The configuration of the electron cloud of an individual porphyrin molecule and its absorption spectrum are very sensitive to the surrounding media due to the number of free anions/cations presented in the solution. The used porphyrin salts after dissolving in deionised water usually had an acidity of about pH 4. The metal-free TPPS molecules in water solution at pH 4 are diprotonated⁹². The deprotonation process of TPPS

molecules in aqueous solution (10⁻⁵ M) was performed by adding NaOH and checked by UV-Vis spectroscopy. The FeTPPS absorption spectrum does not change in the acidity range of 4.0-6.0. The corresponding UV-Vis spectra of as-prepared diprotonated (pH 4), deprotonated (pH6) TPPS solutions and FeTPPS at pH 4 are shown in Fig. 4.4.



solutions was controlled and kept at pH 4 or 6 to avoid any possible formation of TPPS J and H-aggregates and non-stable monoprotinated states in the range of pH 5.0-5.5⁹³. As typical for metalloporphyrins⁹⁴, a Soret band of FeTPPS is blue-shifted to 394 nm and a wide band appears centred at 530 nm⁹⁵. The influence of pH and a central metal atom to the configurations of TPPS and FeTPPS molecules in aqueous solutions are proposed in Fig. 4.5. The proposed molecular configurations of TPPS and FeTPPS at different pH are drawn using HyperChem 5.02 software

The measured Raman spectra of TPPS and FeTPPS films deposited on the glass substrates from aqueous solution are shown in Fig. 4.7. The TPPS (pH 4) mode at 1,477 cm⁻¹ can be assigned to the in-plane motion of the phenyl ring⁹⁶. This mode disappears in the free base as a result of the almost perpendicular orientation of the phenyl rings. These configuration changes also lead to a downshift of the out-of-plane motion of the porphyrin core to 311 cm⁻¹, downshift of totally symmetric pyrrole breathing vibrations from 987 and

1,017 cm⁻¹ to 964 and 1,002 cm⁻¹; upshift of phenyl deformation vibrations to 718 cm⁻¹ and an upshift of C_b-C_b stretch from 1,539 to 1,548 cm⁻¹ after deprotonation is in line with the 'rule of protonation'⁹⁷ for stretching vibrations. These configuration changes also lead to the significant enhancement of pyrrole modes at 810, 1,330 and 1,363 cm⁻¹, C_b-H bending deformations at 1,089 and 1,144 cm⁻¹ and a C_m-phenyl stretching mode at 1,239 cm⁻¹ (see Table 4.1)

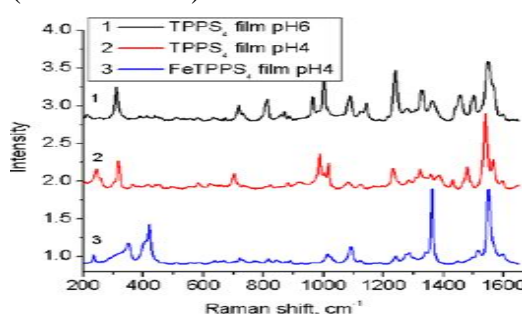


Fig. 4.5. Normalised Raman spectra of diprotonated TPPS (pH 4), non-protonated TPPS (pH 6) and FeTPPS (pH 4) films formed onto the glass substrates (λ_{exc} 532 nm)

Table 4.1. The assignment of Raman bands of TPPS

The mode explanation	TPPS (pH 4)	Changes in TPPS (pH 6)
Out-of-plane motion of the porphyrin core	316 cm ⁻¹	Downshift to 311 cm ⁻¹
Phenyl deformation vibrations	704 cm ⁻¹	Upshift to 718 cm ⁻¹
Symmetric pyrrole breathing vibrations	987 and 1,017 cm ⁻¹	Downshift to 964 and 1,002 cm ⁻¹
Pyrrole modes	810, 1,330 and 1,363 cm ⁻¹	Enhanced peaks
C _b -H bending deformations	1,089 and 1,144 cm ⁻¹	Enhanced peaks
C _m -phenyl stretching mode	1,239 cm ⁻¹	Enhanced peak
Phenyl ring motion	1,477 cm ⁻¹	Disappears
C _b -C _b stretch	1,539 cm ⁻¹	Upshift to 1,548 cm ⁻¹

Because the Raman spectra of FeTPPS spectrum is not being changed in the acidity range of pH 4-6 so only the single spectrum of FeTPPS film (pH 4) is shown. In the case of FeTPPS film, an iron atom could be a cause of another feature in the difference spectrum centred at 420 and 1,362 cm⁻¹, corresponding to the observed

increase of Fe-O-Fe stretching vibrations. The disappearance of the mode at 1,477 cm⁻¹ indicates a rotation of the phenyl rings and on a less protonated state of FeTPPS when the film is formed. The broad peak at 314 cm⁻¹ is relative to the motion of the porphyrin core, and allows the assumption that FeTPPS molecules are strongly deformed after the formation of film.

Characterisation of porphyrin films on CVD graphene

To investigate the graphene impact on porphyrins, the measurements with Raman spectroscopy were performed. The Raman spectrum of a non-protonated TPPS after an interaction with graphene strongly correlated with the one of the film formed on glass substrate Whereas in the case of purchased CVD graphene, which was on a Si surface, during measurements an intensive Si band on 521 cm⁻¹ and second, non-so intensive band around 1,000 cm⁻¹ was visible (Fig. 4.6).

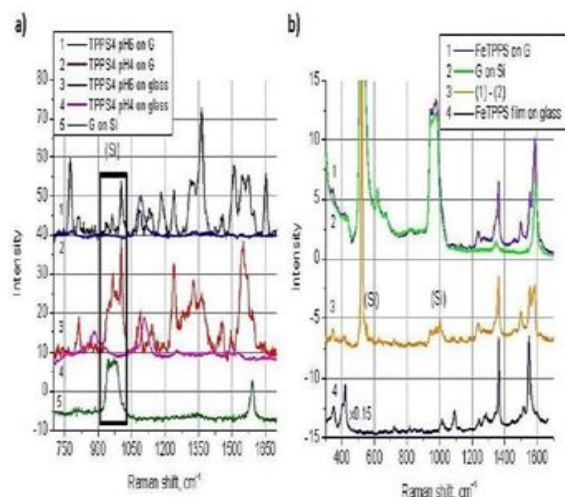


Fig. 4.6. The normalised Raman spectra of a) TPPS and b) FeTPPS on glass and graphene surface (λ_{exc} - 532 nm)

While non-protonated TPPS is adsorbed on graphene, its Raman spectrum differs from the non-protonated film on glass. There is a redistribution in the peak intensities, a

significant enhancement of peaks (1,363, 1,509 cm⁻¹), and even an appearance of new peaks (774, 1,181, 1,653 cm⁻¹) (Fig. 4.8). The sensitive to the protonation ν_2 Cb-Cb stretching mode at 1,548 cm⁻¹ is not shifted, but ν_{11} Cb-Cb stretching mode at 1,510 cm⁻¹ is upshifted and enhanced. Another enhanced band at 1,365 cm⁻¹ can be assigned to pyrrole vibrations which also involve the Cb atom. The mechanism of Raman enhancement on graphene is usually explained by the charge-transfer phenomenon⁹⁸ by analogy with the chemical enhancement mechanism in 'classic' SERS, when an electronic coupling between molecules and metal substrate occurs. The peak at 1,184 cm⁻¹ can be a Raman fingerprint of symmetric phenyl vibrations of desulphonated TPPS, TPP⁹⁹, and should be considered with a rising peak at 1,575 cm⁻¹ assigned to phenyl C=C stretch. It was shown in that the p-sulphonation of TPP phenyl groups causes a weakening of the peak at 1,575 cm⁻¹, and it disappears for TPPS and vice versa, it's strengthening could be evidence of the desulphonation of phenyl rings of non-protonated TPPS. Two other bands, arising at 780 and 1,650 cm⁻¹, can be assigned to significantly enhanced pyrrole vibrations¹⁰⁰.

After interaction of FeTPPS macrocycle with graphene, there were no changes in the peaks, which are related to the vibrations of an iron atom- 417 and 1,364 cm⁻¹. The relative increase of the Cm- phenyl (1,236 cm⁻¹) and Cb-Cb (1,499 cm⁻¹) stretching vibrations together with a significant decrease of the vibrations involving an iron atom (417 and 889 cm⁻¹) correspond to the strong deformation of FeTPPS core after an interaction with graphene and a structural disorder of the film. In the case of both TPPS and FeTPPS a weak Raman signal at 1,477 cm⁻¹ indicates that the phenyl rings are perpendicular to the porphyrin core as shown in Fig. 4.7¹⁰¹.

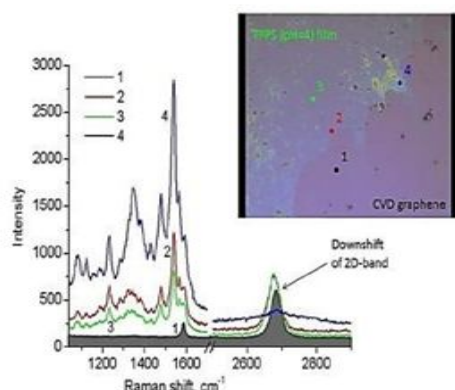


Fig. 4.7. The Raman spectra of TPPS film on CVD graphene in different places (λ_{exc} -532 nm)

The measured thicknesses of uniform films of the different porphyrin solutions adsorbed on chemical vapour deposition (CVD) graphene were typically less than 10 nm (see Fig. 4.8).

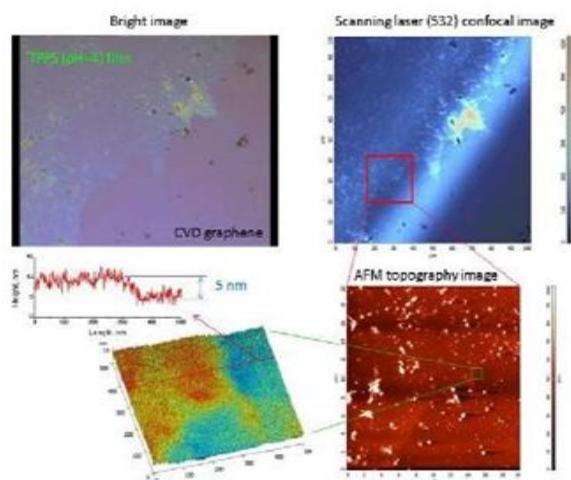


Fig. 4.8. The bright, confocal and AFM images of TPPS film formed on CVD graphene

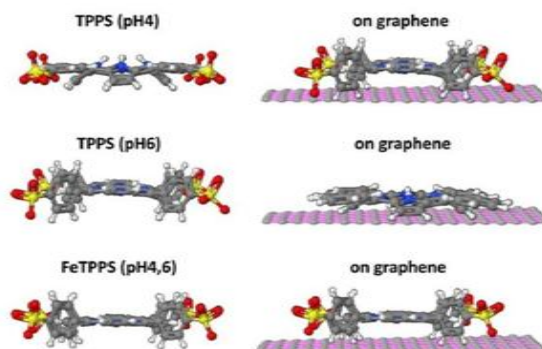


Fig. 4.9. The configurations of TPPS and FeTPPS molecules in aqueous solutions and when adsorbed onto graphene (right)

Graphene oxide functionalisation with hematoporphyrin

A covalent interaction of hematoporphyrin (HP) with functionalised graphene- graphene oxide was investigated. A combination of optical techniques, as UV-Vis absorption, luminescence properties and Raman scattering, can be efficiently used to detect an interfacial structure of hematoporphyrin/graphene oxide (HP/GO) nanoensembles. The stable in aqueous media at neutral pH HP/GO nanocomposites were obtained as a result of the esterification reaction catalysed by sulfuric acid (SA). The nanocomposite with stronger absorption and emission represents a layered structure composed of hematoporphyrin oligomers adsorbed on the surface of GO in a monolayer through covalent, electrostatic and π -stacking interactions. The formation of such hybrid structures, where graphene oxide plays a role of a non-toxic sheet-like nanocarrier, opens the way to create a functional nanocomposite with a high-level of selective emission and efficient photosensitising ability using unique graphene properties.

Characterisation of hematoporphyrin

The configuration of an electron cloud of hematoporphyrin and its absorption spectrum also depends on the surrounding media. The

HP after dissolving in deionised water had an acidity of about pH 7. Under neutral conditions (pH~7), carboxyl groups of hematoporphyrin are mainly deprotonated and become negatively charged; oppositely charged carboxyl groups and amino groups stimulate aggregation of hematoporphyrin molecules¹⁰² (Fig. 4.10). The pH changing process of HP molecules in aqueous solution was performed by adding H₂SO₄ or NaOH and controlling by UV-Vis spectroscopy.

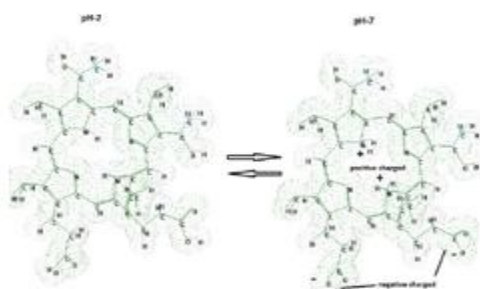


Fig. 4.10. The changes of hematoporphyrin under acidic and neutral pH level

Absorption and emission spectra of hematoporphyrin are presented in Fig. 4.13. The data in Table 4.2 showed that treatment with sulfuric acid essentially changes both the absorption and emission spectra of HP. The specific features of a strong Soret band (position, narrow half-width, strong vibronic coupling, etc.) indicates that at pH~2 a monomer form of HP dominates in the solution. The hypochromic (blue) shift, wide and less intensive absorption bands indicate the aggregation of HP in the aqueous solution at neutral pH~7. The emission spectra of HP at pH~7 show typical fluorescence peaks on 616 nm and 676 nm; after adding sulfuric acid we observed the change of the spectrum with a main peak at 655 nm.

Table 4.2. Absorption and emission range/peaks

	Absorption range, nm	Main absorption peaks, nm	Emission range, nm	Main emission peaks, nm	Interpretation
pH-2	220-585	381, 399, 550	585-750	623, 652, 671	Monomer form
pH~7		367, 390		616, 674	Aggregate form

The observed features are in good agreement with the model that sulfuric acid reduces aggregation of HP and shifts the equilibrium to the monomer form. Under neutral conditions (pH~7), carboxyl groups are mainly deprotonated (the pK_a of carboxyl groups are mainly in the range 4-5), and become negatively charged; oppositely charged carboxyl groups and amino groups stimulate the aggregation of hematoporphyrin molecules. Sulfuric acid changes the pH below pK_a disturbing electrostatic interactions and leads to the disaggregation of HP aggregate.

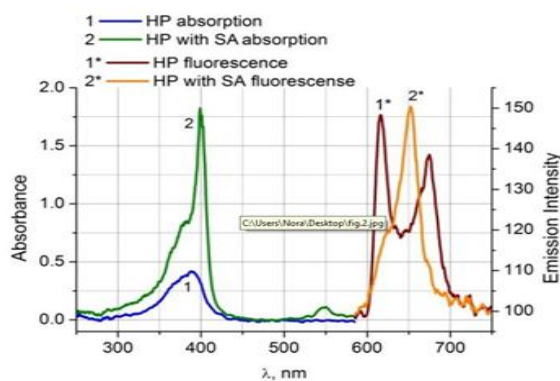


Fig. 4.11. Absorption and emission spectra of hematoporphyrin with and without sulfuric acid, Respectively

Graphene oxide absorption and emission changes under sulfuric acid treatment

The absorption spectrum of GO solution in water ranging from 200 to 800 nm shows a main peak at ~230 nm and a weak shoulder peak at ~302 nm. Typical GO absorption spectra in deionized water are presented in Fig. 4.16. The addition of SA had no

significant influence on GO absorption spectra. Excitation with a blue laser (473 nm) shows low luminescence within the range of 600-700 nm. Owing to the low absorption and emission efficiency as well as structureless spectra of GO within the visible region, only small changes in optical spectra were observed when SA was added to the GO solution¹⁰³.

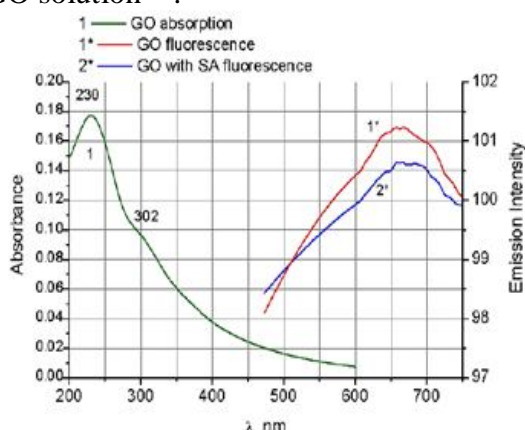


Fig. 4.12. Absorption spectra of GO and emission spectra of GO with and without SA

Within one hour after adding SA some visible macroscopic aggregation within GO solutions may be seen with the naked eye. Typical Raman scattering spectra of the GO films treated with and without SA are presented in Fig. 4.13 within the regions of the in-phase vibration of the GO lattice (G/2G band) at c.a. 1,600/3,200 cm⁻¹ and the disorder band caused by the GO edges (D/2D band) at approximately 1,334/2,668 cm⁻¹. The decreasing of D/G ratio at low pH as well as G band shift to the high energy indicates the decreasing of the defects and formation of more ordered structure¹⁰⁴.

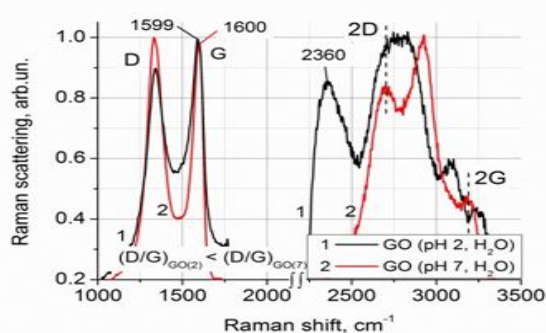


Fig. 4.13. The typical Raman spectra of GO treated with SA (λ_{ex} - 532 nm)

Synthesis of supramolecular structures using graphene oxide Graphene oxide functionalisation with doxorubicin

A covalent interaction of GO with anticancer drug doxorubicin (DOX) was investigated. The nano- and microcomposites composed of doxorubicin adsorbed on the surface of GO through covalent and non-covalent interactions such electrostatic and π - π stacking interactions. The formation of such hybrid and three-dimensional structures open the way to create a functional nano- and microcomposite, where graphene oxide plays a role of a non-toxic nanocarrier and of a substance which enhances the anticancer effect. The functionalisation process of GO with DOX were determined by UV-Vis spectrophotometer, Raman spectroscopy and atomic force microscopy. DOX was covalently attached on carboxylated GO by the covalently linkage of the carboxyl group with the amino group, with heating and ultrasonification for one hour to accelerate the reaction (GO/DOX). The reaction is showed below:



UV-Vis and Raman characterisation of GO/DOX

As shown in Fig. 4.14 the doxorubicin (20 μ g/ml) has a peak of plasmon absorbance at 488 nm¹⁰⁵. While when the concentration of DOX was only 2 μ g/ml - no peak was observed, nor in mix with the GO. The UV-Vis spectra of GO show the main peak at 252 nm due to the C=C bond in an aromatic ring, the red-shift of the absorption is due to the deoxygenation reaction, whereas the broad shoulder peak at 302 nm can be assigned to C=O. The absorption over 302 nm is expected to be caused by the conjugated

fused ring plane¹⁰⁶. Shaoling Wu (2013) studied absorption properties of doxorubicin onto graphene oxide: equilibrium, kinetic and thermodynamic. The thermodynamic studies indicate that the adsorption of DOX on GO is spontaneous and endothermic in nature¹⁰⁷.

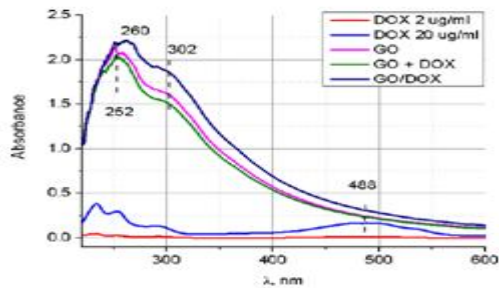


Fig. 4.14. The absorption spectra of GO, DOX, mixed GO+DOX and GO/DOX

When DOX was covalently conjugated on GO, the absorption peak of GO/DOX is shifted to 260 nm. As to the fluorescence spectra (Fig. 4.27), GO and DOX (GO+DOX) mix have the fluorescence peak on 643 nm as free DOX, though the fluorescent intensity diminished due to the quenching effect of GO. These optical results indicated that DOX had been loaded on the GO based nanocarrier as expected (Huang et al., 2013). After the heating and mixing (when DOX was covalently attached to GO) of this solution a bathochromic shift was observed, - the main peak shifted to 647 nm. The fluorescent spectrum results also indicate that a strong π - π stacking interaction exists between GO and DOX¹⁰⁸.

Graphene oxide has a couple of Raman-active bands on the in-phase vibration of the graphene oxide lattice (G band) as well as the disorder band caused by the graphene oxide edges (D band). The visible decrease in amplitude could be caused by decreasing the number of free hydroxyl groups after mixing with DOX. The shift to 1,351 cm^{-1} and increasing in amplitude after covalent binding of DOX may be caused by the appearance of different type of groups, the amide linkage and increasing number of

defects on graphene oxide lattice. The G band shift from 1,589 to 1,594 cm^{-1} indicates the deformation of ordered structure. The appearance of new peaks, the 1,500 cm^{-1} indicates the stretching vibration of C-N109 bond and two peaks 1,737 and 1,786 cm^{-1} , the stretching vibrations of the C=O bond (Fig. 4.15).

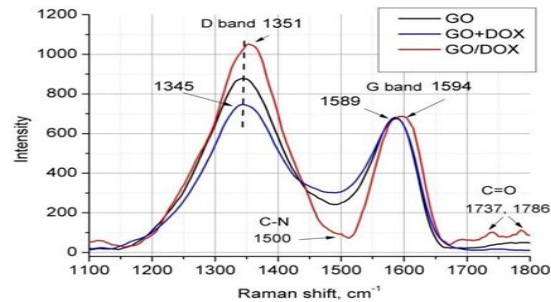


Fig. 4.15. The Raman spectra of GO, mixed GO+DOX and GO/DOX (λ_{ex} - 532 nm)

AFM and SEM characterisation of GO/DOX

To clarify the formation of GO/DOX composites AFM and SEM measurements was performed. The AFM picture showed the possible formation of GO/DOX filaments (Fig. 4.16).

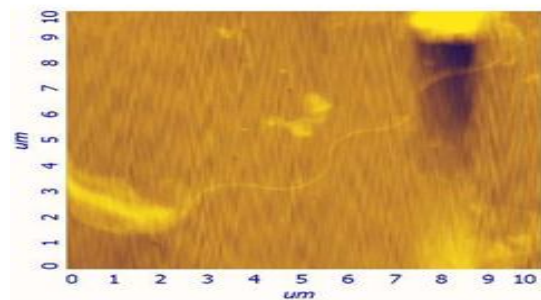


Fig. 4.16. The height picture of GO/DOX aggregate

SEM measurements confirmed the formation of different sizes of filaments. The diameter of big filaments is around 15-20 μm (Fig. 4.17, a) and the middle size filaments are around 5-10 μm (Fig. 4.17, b). The dimensions of the “new-born” are about 1 μm diameter, and 2-3 μm length (Fig. 4.17, c).

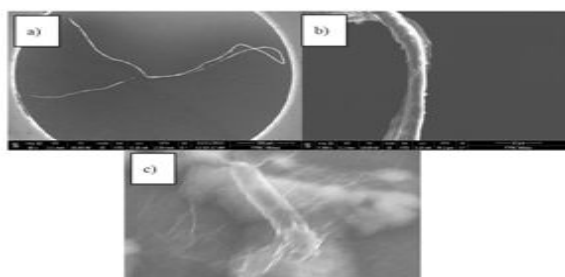
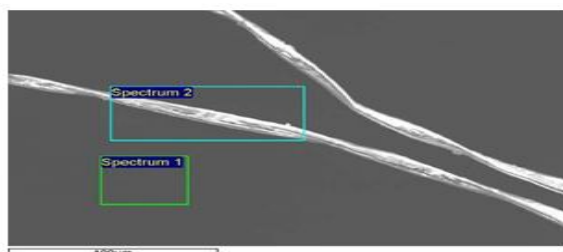


Fig. 4.17. The SEM pictures of different size of GO/DOX filaments

The possible formation of filament forms a mass, consisting of graphene oxide and doxorubicin

Fig. 4.18. SEM picture of composites based GO and DOX



Spectrum 1 proves the Si surface, accordingly spectrum 2 proves that the filaments were based mainly from doxorubicin (according to the Brutto formula DOX- C₂₇H₂₉NO₁₁), but some mismatches with amounts of oxygen (8.41 instead of 15.51) and carbon (34.92 instead of 38.07) show that another material, graphene oxide, had an influence in this formation (Fig. 4.18, Table 4.4)

Table 4.4. EDX analysis of composites based on GO and DOX

Results in atomic%	C	N	O	Si	S
Spectrum 1	5.01	0.45	1.21	93.13	0.19
Spectrum 2	34.92	1.41	8.41	55.27	0.01

Conclusions

The protonation of porphyrin macrocycle or the existence of a central metal atom for the TPPS family plays an important role in the molecular conformation and orientation when

interacting with single-layer graphene (see Fig. 4.11). The interaction of diprotonated metal-free TPPS with graphene leads to the deprotonation process of the porphyrin macrocycle. The downshifts of G and 2D Raman peaks of graphene after an interaction directly imply a charge transfer from TPPS molecules to graphene resulting in the electron doping of graphene, but the Raman enhancement factors are relatively low. The existence of a central metal atom in the porphyrin macrocycle (iron) is important in the integrity of the FeTPPS molecule during an interaction, but results in the decreased Raman signals in spite of the observed charge transfer effect. Initially deprotonated TPPS undergoes the atomic changes after an interaction with graphene, which leads to the appearance of new Raman bands and at least one order of magnitude higher enhancement factor for some pyrrole modes. The proposed explanation of enhancement is that a strong interaction is realised through the pyrrole and planar desulphonated phenyl rings of a closely located TPPS molecule on a single-layer graphene surface. A variety in the central metal atom of porphyrin macrocycle or its protonation opens wide opportunities for the fabrication of novel composite graphene-porphyrin nanomaterials with predetermined properties.

It was found that advanced macromolecules using graphene-based material, graphene oxide and anticancer drug- doxorubicin could be formed. The obtained results validated the concept of using covalent linkage of the carboxyl group from GO with the amino group from doxorubicin. The GO/DOX mixture led to the reduction of the DOX concentration in drugs with the purpose of reducing the undesirable side-effects and could be used as a drug-drug delivery system for healing tumours and future theranostics.

Reference:-

1. Loh, Kian Ping, et al. "Graphene oxide as a chemically tunable platform for optical applications." *Nature chemistry* 2.12 (2010): 1015.
2. Pan, Dengyu, et al. "Hydrothermal route for cutting graphene sheets into blue-luminescent graphene quantum dots." *Advanced materials* 22.6 (2010): 734- 738.
3. Pimenta, M. A., et al. "Studying disorder in graphite-based systems by Raman spectroscopy." *Physical chemistry chemical physics* 9.11 (2007): 1276-1290.
4. Kudin, Konstantin N., et al. "Raman spectra of graphite oxide and functionalized graphene sheets." *Nano letters* 8.1 (2008): 36-41.
5. Cançado, L. G., et al. "General equation for the determination of the crystallite size L_a of nanographite by Raman spectroscopy." *Applied Physics Letters* 88.16 (2006): 163106.
6. Ferrari, Andrea C., et al. "Raman spectrum of graphene and graphene layers." *Physical review letters* 97.18 (2006): 187401.
7. Ni, Zhenhua, et al. "Raman spectroscopy and imaging of graphene." *Nano Research* 1.4 (2008): 273-291.
8. GONÇALVES, P. J., et al. Effect of protonation on the photophysical properties of meso-tetra (sulfonatophenyl) porphyrin. *Chemical Physics Letters*, 2005, 407.1: 236-241
9. Kelbaskas, L., et al. "Excitation relaxation and structure of TPPS4 J-aggregates." *Journal of luminescence* 101.4 (2003): 253-262.
10. Horváth, Ottó, et al. "Photophysics and photochemistry of kinetically labile, water- soluble porphyrin complexes." *Coordination chemistry reviews* 250.13-14 (2006): 1792-1803.
11. Gonçalves, P. J., et al. "Excited state dynamics of meso-tetra (sulphonatophenyl) metalloporphyrins." *The Journal of Physical Chemistry A* 112.29 (2008): 6522- 6526.
12. Friesen, Benjamin A., et al. "New nanoscale insights into the internal structure of tetrakis (4-sulfonatophenyl) porphyrin nanorods." *The Journal of Physical Chemistry C* 113.5 (2009): 1709-1718.
13. Akins, Daniel L., Han-Ru Zhu, and Chu Guo. "Aggregation of tetraaryl-substituted porphyrins in homogeneous solution." *The Journal of Physical Chemistry* 100.13 (1996): 5420-5425.
14. Huang, Jie, et al. "Mechanism of cellular uptake of graphene oxide studied by surface-enhanced raman spectroscopy." *Small* 8.16 (2012): 2577-2584.
15. Bolyard, Chelsea, et al. "Doxorubicin synergizes with 34.5 ENVE to enhance antitumor efficacy against metastatic ovarian cancer." *Clinical Cancer Research* 20.24 (2014): 6479-6494.
16. Xu, MingSheng, et al. "Unique synthesis of graphene-based materials for clean energy and biological sensing applications." *Chinese science bulletin* 57.23 (2012): 3000-3009.
17. Buchner, Florian. *STM Investigation of Molecular Architectures of Porphyrinoids on a Ag (111) Surface: Supramolecular Ordering, Electronic Properties and Reactivity*. Springer Science & Business Media, 2010.
18. Marchetti, J. M., and A. F. Errazu. "Esterification of free fatty acids using sulfuric acid as catalyst in the presence of triglycerides." *Biomass and Bioenergy* 32.9 (2008): 892-895.
19. Shang, Jingzhi, et al. "The origin of fluorescence from graphene oxide." *Scientific reports* 2 (2012): 792.
20. Kudin, Konstantin N., et al. "Raman spectra of graphite oxide and functionalized graphene sheets." *Nano letters* 8.1 (2008): 36-41.

21. HUANG, Jie, et al. Tracking the intracellular drug release from graphene oxide using surface-enhanced Raman spectroscopy. *Nanoscale*, 2013, 5.21: 10591-10598
22. Zhang, Weiyang, et al. "Enhancement of photocatalytic H₂ evolution of eosin Y-sensitized reduced graphene oxide through a simple photoreaction." *Beilstein journal of nanotechnology* 5.1 (2014): 801-811.
23. Wu, Shaoling, et al. "Adsorption properties of doxorubicin hydrochloride onto graphene oxide: equilibrium, kinetic and thermodynamic studies." *Materials* 6.5 (2013): 2026-2042.
24. Yang, Xiaoying, et al. "High-efficiency loading and controlled release of doxorubicin hydrochloride on graphene oxide." *The Journal of Physical Chemistry C* 112.45 (2008): 17554-17558.
25. Hannemann, Klaus, and Friedrich Seiler, eds. *Shock Waves: 26th International Symposium on Shock Waves*. Vol. 1. Springer Science & Business Media, 2009.